The impact of long-term changes in ocean waves and storm surge on coastal shoreline change: A case study of Bass Strait and south-east Australia

Mandana Ghanavati[1], Ian R. Young*[1], Ebru Kirezci[1], Jin Liu[1]

[1]Department of Infrastructure Engineering, University of Melbourne, Melbourne, VIC 3010, Australia.
* Corresponding author: ian.young@unimelb.edu.au

Abstract

Numerous studies have demonstrated that significant global changes in wave and storm surge conditions have occurred over recent decades and are expected to continue out to at least 2100. This raises the question as to whether the observed and projected changes in waves and storm surges, will impact coastlines in the future? Previous global-scale analyses of these issues have been inconclusive. This study investigates the south-east coast of Australia over a period of 26 years (1988-2013). Over this period, this area has experienced some of the largest changes in wave climate of any coastal region, globally. The analysis uses high-resolution hindcast data of waves and storm surge, together with satellite observations of shoreline change. All datasets have been previously extensively validated against in situ measurements. The data are analysed to determine trends in each of these quantities over this period. The coastline is partitioned into regions and spatial consistency between trends in each of the quantities investigated. The results show that beaches along this region appear to have responded to the increases in wave energy flux and changes in wave direction. This has enhanced non-equilibrium longshore drift. Long sections of the coastline show small but measurable recession before sediment transported along the coast is intercepted by prominent headlands. The recession is largest where there are strong trends of increasing wave energy flux and/or changes in wave direction, with recession rates of up to 1m/year. Although a regional study, this finding has global implications for shoreline stability in a changing climate.

1. Introduction

Sandy coastlines are dynamic systems, responding to changes in waves, storm surge, sea level, available coastal sediment supply and human activities (e.g. coastal structures, beach nourishment) (Komar, 1998; Masselink, et al., 2016). These changes occur on a variety of spatial and temporal scales. Spatially, changes in beach alignment and the presence of coastal shoreline features (headlands and bays) impact both the wave climate for individual beaches and the characteristics of longshore drift. At temporal scales of days, beach erosion results from individual storms (Komar, 1998; Harley, et al., 2017; Masselink, et al., 2016). At time scales of 2 to 10 years, changes in storminess associated with climate indices (e.g. El Niño) (Ranasinghe, et al., 2004; Harley, et al., 2011; Barnard, et al., 2015; Vos, et al., 2023) can result in sustained impacts on beach systems. Longer term changes in mean sea level as a result of climate change are also predicted to result in coastal recession (Hinkel, et al., 2013; Ranasinghe, 2016; Vousdoukas, et al., 2020; Ranasinghe, et al., 2021; Vitousek, et al., 2023). It should be noted that throughout this paper

39 we refer to shorter-term changes in beach location due to storms or a series of storms as erosion
40 or accretion. Longer-term changes such as those due to climate change are referred to as recession
41 or progradation.

42 Waves and storm surges are generated by environmental variables (wind and sea level pressure
43 gradient). It has been shown that these environmental variables are impacted by climate change
44 and hence long-term historical changes (trends) in waves (Wang & Swail, 2001; Wang, et al.,
45 2009; Hemer, 2010; Young, et al., 2011; Aydoğan & Ayat, 2018; Zheng & Li, 2017; Young &
46 Ribal, 2019; Takbash & Young, 2020; Reguero, et al., 2019; Cao, et al., 2021; Young & Ribal,
47 2022; Liu, et al., 2022; Morim, et al., 2022; Erikson, et al., 2022) and storm surges (Paprotny,
48 2014; Androulidakis, et al., 2015; Cid, et al., 2016; Muis, et al., 2016; Kim, et al., 2017; Feng, et
49 al., 2018; Ghanavati, et al., 2023) have been observed. A number of studies have also projected
50 continued global increases (positive trends) in wave height over the 21st century, particularly in
51 the Southern Hemisphere, under plausible climate change scenarios (Hemer, et al., 2013; Meucci,
52 et al., 2020; Hochet, et al., 2021; Liu, et al., 2022; Meucci, et al., 2023; Morim, et al., 2023; Liu,
53 et al., 2023).

54 If sandy coasts are impacted by changes in wave and storm surge conditions, the potential for
55 continued increases in the values of these variables in the future raises the question as to what
56 impact this may have on sandy coastlines and associated communities. As a means of determining
57 potential future impacts, the obvious precursor is to assess the impacts that historical changes in
58 long-term wave and storm surge conditions have had on coastlines. In the first study of its type,
59 Ghanavati, et al. (2023) investigated this issue at global scale by using long-term modelled wave
60 and storm surge data together with satellite observations of beach recession/progradation over the
61 last 30 years. They found that, noting the relatively small trends in wave and storm surge conditions
62 over this period, the accuracy of the available data, and other unrelated impacts on shoreline
63 response (e.g. availability of sediment, human impacts), no clear relationship was evident.

64 In order to address the limitation of the Ghanavati, et al (2023) work, the present study examines,
65 in much finer detail, the south-east coastline of Australia. This is an area where long-term trends
66 in wave conditions are some of the largest in the world, responding to changes in wave climate in
67 the Southern Ocean (Liu, et al., 2022). Therefore, if there is a causal link between changes in long-
68 term wave and storm surge climate and shoreline response, one would expect clear signs in this
69 region. As a regional area is considered, it is possible to use higher resolution data (both model
70 and satellite) removing uncertainties in the global-scale Ghanavati, et al (2023) study. In addition,
71 the regional-scale study enables an analysis of the role beach compartments play in defining
72 sediment transport. As such, one can investigate changes in longshore drift due to changes in wave
73 climate and the characteristic signature of such non-equilibrium transport with eroding beaches
74 and deposition of sediment behind peninsulas.

75 Although the present study is regional, the area being studied is a proxy for the potential impacts
76 one may see in other regions of the world as changes in wave and storm surge climate are projected

77 to continue to change in the future. Hence, the findings of the study have global implications for
78 shoreline response in the future. The study is unique in that it has been possible to combine high
79 resolution datasets for waves, storm surge and shoreline response and addresses a previously
80 unexplored area of shoreline response in a changing climate.

81 The structure of the paper is as follows. Section 2 outlines the study area, data sets and analysis
82 techniques used in the study. Results are given in Section 3, including the observed relationships
83 between changes in wave and storm surge quantities and beach recession/progradation. Discussion
84 and conclusions are provided in Section 4.

85

2. Methodology

2.1 Study Area

89 The study region is shown in Figures 1 and 2, and covers an area of 137E°–155°E, 35S°–45°S.
90 Three Australian coastal states span this domain, Victoria, southern New South Wales and the
91 island of Tasmania in the south of the domain. The south-eastern coast of the mainland of Australia
92 (Victoria), the coastal area of the study, is separated from Tasmania by the relatively shallow Bass
93 Strait. The area is exposed to a particularly complex wave climate (Liu, et al., 2022). To the west,
94 the coast is exposed to the Southern Ocean and hence experiences a very energetic wave climate
95 with recorded significant wave height as high as 10m (Meucci, et al., 2023). The wave climate of
96 this region is dominated by south-westerly Southern Ocean swell. Central regions of the study
97 domain are protected by the island of Tasmania and have a mixed wave climate with swell from
98 both the south-west and south-east and locally generated wind sea. To the east, the wave climate
99 is more heavily dependent on the local wind-sea but with south-easterly swell still playing a role
100 (Liu, et al., 2022).

101

102 Both observational data from satellite altimeters (Young, et al., 2011; Young & Ribal, 2019;
103 Timmermans, et al., 2020) and model hindcasts (and reanalyses) (Cao, et al., 2021; Young & Ribal,
104 2022) show that over the last 35 years, there has been a small global increase in mean significant
105 wave height. This increase is largest in the Southern Ocean (approximately 3mm/year or an
106 increase of 3% over the last 30 years), which results in impacts across the Indian, South Pacific
107 and South Atlantic Oceans due to radiating swell. Therefore, the study area is a location where
108 relatively large changes in significant wave height have occurred over the period.

109

2.2 Datasets

111 This study uses regional datasets for each of wave, storm surge, and coastal change from which
112 the historical trend magnitudes of the various quantities were calculated. The datasets under
113 consideration cover different periods of time, and thus, to ensure consistency across analyses, a

114 common time period from 1988 to 2013 was selected. A description of each dataset used in the
115 study is provided below.
116
117 _Liu et al. (2022) regional wave hindcast_ is a high-resolution regional wave hindcast dataset based
118 on a WAVEWATCH III model with an ST6 physics package (Liu, et al., 2021). The regional
119 model covers the domain shown in Figure 2 using an unstructured grid with a coastal resolution
120 as small as 500m and a coarser deep water resolution as large as 10km. The regional model is
121 nested within a global model using the same ST6 physics (Liu, et al., 2021). Both the regional and
122 global models are forced with ERA5 winds (Hersbach, et al., 2020). The regional wave model
123 dataset has been extensively validated (Liu, et al., 2022; Liu, et al., 2023) against both a network
124 of coastal buoys and satellite altimeter data. Wave data were available from the hindcast with a
125 temporal resolution of 1 hour. The period of the hindcast was from 1981 to 2020. The dataset's
126 high resolution is particularly important for studying coastal regions, where wave conditions can
127 vary significantly over short distances. Additionally, the long period of coverage allows us to
128 identify and analyze trends in the wave climate over several decades, providing insight into the
129 possible effects of historical climate change on the region.
130
131 _Colberg, et al. (2018) Australian water level hindcast_ is a dataset of sea level simulations for the
132 Australian coastline. The dataset was generated using the Regional Ocean Modelling System
133 (ROMS) (Shchepetkin & McWilliams, 2005), which was run in a depth-integrated form on a 5 km
134 resolution grid for the Australian region. Tidal currents and heights at open boundaries were
135 specified from the TPXO7.2 global model (Egbert & Erofeeva, 2002). TPXO7.2 best fits (in a
136 least squares sense) the Laplace tidal equations and along track averaged data from
137 TOPEX/Poseidon and Jason altimetry data. The ROMS model was run for the period 1981-2013
138 and was forced with NCEP Climate Forecast System Reanalysis (CFSR) (Saha, et al., 2010) wind
139 and surface pressure data. The model has been validated at 14 tide gauge locations around the
140 Australian coastline (Colberg, et al., 2018). Again, the output was available on an hourly basis.

141 _Bishop-Taylor et al., (2021) Geoscience Australia beach dataset_ is a high-resolution regional
142 dataset of shoreline change rate for the coast of Australia. The dataset utilizes a combination of
143 satellite visual data and tidal modelling to map shoreline change, with an along-coast resolution of
144 30m for non-rocky (sandy or muddy) areas. The dataset provides annual values of the shoreline
145 position over the period 1988 to 2019. The dataset has been extensively validated using in-situ
146 measurements, comprising 330 validation transects, each spanning over 10 years of coastal
147 monitoring data. The Mean Absolute Error (MAE) in the trend across these validation points was
148 0.35 m/year (Bishop-Taylor, et al., 2021).

149 ### _2.3_ _Trend calculation_

150 Each of the datasets (waves, storm surge, shoreline location) are defined at different resolution and
151 in different manners (structured and unstructured grids, specific shoreline positions), therefore
152 none of these quantities are co-located. As shown by Ghanavati, et al., (2023) and subsequently

153 confirmed in Figures 3, 4 and 5, trends in both wave height and storm surge quantities generally
154 vary smoothly along extended coastal regions (100s of kilometres). Shoreline
155 recession/progradation rate can, however, vary rapidly in magnitude and sign over relatively short
156 spatial scales (10s of kilometres) (Luijendijk, et al., 2018; Ghanavati, et al., 2023). That is, one
157 beach can be receding whilst the next is prograding. As such, simple scatter plots of rates of change
158 of wave and storm surge quantities verses recession/pogradation rates are not meaningful. Rather,
159 one needs to consider relationships over spatial regions of the coastline. To achieve such an
160 analysis, we divide the study domain in Figure 1 into six regions, each spanning 2° in longitude –
161 (a) 138E°-140E°, (b) 140E°-142E°, (c) 142E°-144E°, (d) 144E°-146E°, (e) 146E°-148E° and (f)
162 148E°-150E° from west to east. These regions span the differing wave climates of the study
163 domain (see Figure 2 and subsequent discussion). For analysis purposes, we present data as
164 follows. Wave quantities are presented both as colour shaded plots, and at shoreline locations
165 corresponding to ocean points defined by the unstructured WAVEWATCH III computational grid.
166 Storm surge quantities are shown at the locations corresponding to the ocean points nearest the
167 land/sea transition of the ROMS 5km computational grid. Coastal change points are as defined at
168 coastal locations in the Bishop-Taylor et al., (2021) dataset, which has an along-cost resolution of
169 30m.

170 Each of the three datasets used in the study covers a different period of time: wave hindcast - 1981
171 to 2020, storm surge data - 1981 to 2013, and shoreline change data - 1988 to 2019. To ensure a
172 consistent evaluation of the trends and variability in the oceanic parameters, a common analysis
173 period of 1988 to 2013 was selected for the study.

174 For each of the datasets, a range of quantities to be investigated were calculated. These include:
175 waves – mean significant wave height (H_s), 95th percentile significant wave height (H_s^{95}), mean
176 wave energy flux ($C_g E$), mean wave period (T_m) and mean wave direction (θ_m), where C_g is the
177 group velocity of waves and $E = H_s^2 / 16$ is the wave energy. The hourly data from the regional
178 wave model was used to calculate annual values of each of these quantities.

179 As noted above, various datasets have different temporal and spatial resolutions and hence slightly
180 different approaches were used to evaluate the variability and extremes of oceanic parameters. The
181 wave and surge time series were collected at a temporal resolution of 1 hour, while the shoreline
182 dataset provided annual shoreline change with reference to the shoreline location in 2019.
183 Therefore, annual mean values of wave parameters including significant wave height, wave energy
184 flux, wave direction and wave period were calculated. Furthermore, the extremes were determined
185 by calculating annual higher percentiles (95th, 98th, and 99th) for significant wave height and
186 surge level. These metrics provide a consistent basis for evaluating the variability and extremes of
187 the oceanic parameters across different datasets. As the various percentile thresholds gave similar
188 results, extreme events were determined as occasions on which the time series exceeded the 95th
189 percentile but with such events separated by a minimum of 48 hours. The number of such events

190   in each year were defined as $N_{H_s^{95}}$. In a similar fashion, storm surges were defined as occasions

191   when the water surface elevation, η, exceeded the 95th percentile (η^{95}) and the number of such

192   events was defined as $N_{\eta^{95}}$. Again, annual values of these quantities were determined. The annual

193   values of shoreline position from the Bishop-Taylor et al. (2021) data were defined in a similar

194   manner and represented as C_{GA}.

195   The annual values of each quantity were then used to determine linear trends over the period 1988-
196   2013. Both linear regression and the non-parametric Tiel-Sen estimator (Sen, 1968) were used for
197   this purpose. As the resulting values were very similar, the Sen slope estimates are used in the
198   subsequent analysis. The resulting trend values are represented as: ΔH_s, ΔH_s^{95}, $\Delta C_g E$, $\Delta \theta_m$,

199   $\Delta N_{H_s^{95}}$; $\Delta \eta^{95}$, $\Delta N_{\eta^{95}}$; ΔC_{GA}.

200

201   **3. Results**

202   ***3.1 Wave climate***

203   Figure 2 shows the mean wave climate of the study area and how it has changed over the period
204   1988 to 2013 as indicated by the Liu, et al. (2022) hindcast. Figures 2a and 2b show the mean

205   significant wave height $\bar{H}_s$ and wave energy flux, $\overline{C_g E} = \rho g^2 H_s^2 T_m / (64\pi)$, respectively. As

206   noted above, the significant wave height and wave energy flux vary significantly across the study

207   area. In the west, the coastline is exposed to energetic Southern Ocean swell with mean H_s of

208   approximately 3m. In the eastern regions of the study area, where there is protection provided by

209   the island of Tasmania, mean H_s decreases significantly to less than 1.5m, a decrease by a factor

210   of approximately 2. The wave energy flux shows an even more significant change, with mean
211   values varying from approximately 60kW/m in the west to 15kW/m in the east, a factor of 4. The
212   substantial reduction in wave energy flux is attributed to the protection provided by the island of

213   Tasmania, which leads to a decrease in both H_s and T_m. As shown by Liu, et al. (2022), the

214   mean/peak wave direction also changes significantly across the domain. In the west, the dominat
215   wave direction is defined by energetic south-westerly swell. In the east, the protection provided by
216   the island of Tasmania means that swell entering the area is predominately from the south-east.

217   The changes in wave climate over the study period are also significant across this region. As noted
218   above, a range of studies have shown that the Southern Ocean wave climate has increased over the
219   past 35 years (Young, et al., 2011; Young & Ribal, 2019; Cao, et al., 2021; Young & Ribal, 2022).
220   Swell from the Southern Ocean dominates the western areas of the study region and hence there

221   have been significant changes in the wave climate, as shown by Figures 2c-h. In the west, H_s has

222   increased by approximately 5% (Figure 2c) over the study period and $C_g E$ by approximately 14%

223   (Figure 2d). In contrast, in the east, where the wave climate is not as exposed to Southern Ocean

swell, these values decrease to approximately zero (no change). Figures 2e and f clearly show that the positive trends in H_s are due to changes in both swell and local wind-waves. Figure 2g also shows that there have been only small changes in T_m across the domain.

The most dramatic changes in wave climate concern the mean wave direction, θ_m. Over the western regions of the study domain, there has been a small counter-clockwise rotation of the mean wave direction (less than 1.5°). This is a result of the gradual southward movement of Southern Ocean low pressure systems over recent decades (Morim, et al., 2022). This small change in deep water wave direction, significantly impacts the shadow region in the lee of Tasmania and hence the wave direction, resulting in much larger counter-clockwise rotations of approximately 5° (Figure 2h). These values reduce towards the coast of mainland Australia (eastern area of study region) but are still larger than 3°.

3.2 Storm Surge Climate

As noted above, storm surges were defined as events where the water surface elevation exceeded the 95th percentile value, η^{95}. Figure 3 and 4 show plots for each of the sub-regions referenced in Figure 1. These figures show colour contoured values of $\Delta C_g E$ (Figure 3) and $\Delta \theta_m$ (Figure 4), coastal values of $\Delta \eta^{95}$ and ΔC_{GA}. In contrast to the wave climate, changes in storm surge, $\Delta \eta^{95}$ are very consistent along the coastline of the study area. Values of $\Delta \eta^{95}$ are negative along the entire coastline, decreasing in magnitude from approximately -0.3cm/year in the west to -0.2cm/year in the east. The fact that the magnitude of storm surges has been decreasing over this period is consistent with the observations of Liu, et al. (2023) that as Southern Ocean low pressure systems move south, they increase the mean atmospheric pressure and reduce the pressure gradient over southern Australia. As surface pressure (and wind) drives storm surge, this results in a tendancy for a reduction in the magnitude of storm surges.

3.3 Relationship between waves, storm surge and shoreline change

As previously shown at global scale by Luijendijk, et al. (2018) and Ghanavati, et al. (2023), recession/progradation rates vary in magnitude and sign on relatively small spatial scales. This is because sediment transport can be both offshore/onshore as well as longshore. In the case of non-equilibrium longshore transport of sediment, one would expect some beaches to recede whilst other receive sediment from these beaches and hence prograde. Ghanavati, et al. (2023) speculated that coastlines which show such non-equilibrium behaviour may be responding to long-term changes in the environmental forcing provided by trends in waves and storm surge. A causal relationship is, however, complicated by other variables which may have a larger impact on beach position. These additional factors include the availability of sediment supplied to beach compartments from fluvial sources and the impacts of human-induced interventions such as coastal

259 structures and beach nourishment (Ranasinghe, 2016). Ghanavati, et al. (2023) limited
260 recession/progradation data to values in the range ±1m/year to confine the datasets to changes
261 which may be a result of long-term processes rather than fluvial and human-induced influences,
262 which tend to be much larger in magnitude (Luijendijk, et al., 2018).

263 Therefore, following these precedents, in Figures 3 – 6, the quantity ΔC_{GA} has been filtered to retain
264 only values in the range ±1m/year. Figure 5 shows values of ΔC_{GA} (in the range ±1m/year) as a
265 bar chart along the coastline from 138E° to 150E°. Each of the 2° regions shown in Figures 1, 4
266 and 5 is marked along the longitude axis. As expected, values of ΔC_{GA} in Figures 3, 4 and 5 show
267 both positive (progradation) and negative (recession) values. To quantify recession/progradation,
268 values of ΔC_{GA} in the range -0.05m/year to -1.00m/year are clasified as recession, values in the
269 range +0.05m/year to +1.00m/year as progradation and values in the range ± 0.05m/year as
270 representing stable coastlines. Table 1 shows the percentage of coastal locations classified as
271 receding, prograding or stable under these criteria. In addition, Figure 6 shows histograms of the
272 distribution of the magnitudes of the values of ΔC_{GA}.

273 Table 1 and Figure 6 show that the sections (c) 142E°-144E° and (f) 148E°-150E° are
274 predominately receding. Segment (d) 144E°-146E° shows quite large values of both recession and
275 progradation (see Figure 5) but with more locations prograding than receding. However, this
276 region is complicated by the presence of Port Phillip Bay. The other segments (a), (b) and (e)
277 show no clear difference between the percentage of receding and prograding locations.

278 To understand the results shown in Table 1, we consider each of the two degree sections shown in
279 Figures 3, 4 and 5. In these figures, values of the trend in wave energy flux, $\Delta C_g E$ (Figure 3) or
280 wave direction, $\Delta \theta_m$ (Figure 4) are shown as colour shaded contours over the regions. The trend
281 in storm surge (always negative) are shown as colour coded squares at 5km intervals along the
282 shoreline, at the resolution of the water level model. The satellite-derived values of trend in
283 shoreline location at each beach location (Bishop-Taylor, et al., 2021) are shown as colour coded
284 filled circles, at the 30m along-coast resolution.

285 Figures 3a and 4a show the region from 138E° to 140E° (segment (a), Victor Harbour to Cape
286 Jaffa). This region shows relatively small positive values of $\Delta C_g E$ (approximately 0.01kWm⁻
287 ¹/year) and a small counter-clockwise rotation of the mean wave direct (approximately
288 -0.02deg/year or 0.6° over 30 years). In response to these small changes in wave properties there
289 is no consistent changes in shoreline. In the western regions (138.6E°-139.2E°) the shoreline is
290 prograding. However, this may be associated with fluvial sediments, as this region is the ocean
291 entrance of Lake Alexandrina and the mouth of the Murray River. These results are consistent with
292 the bar chart of Figure 5 and the results in Table 1 and Figure 6a that there is no clear difference
293 between recession and progradation for segment (a).

294 Moving east to segment (b), values of $\Delta C_g E$ increase (Figure 3b) and the region shows small

295 receding shorelines (139.6E°- 141.0E°). This changes to progradation between 141.0E°-141.2E°,

296 west of Cape Bridgewater. This behaviour is consistent with sediment being moved along the

297 shoreline west to east from 139.6E°- 141E° by the increasing wave energy flux and the prevailing

298 wave direction from the south-west. This sediment transport is interrupted by Cape Bridgewater

299 resulting in the progradation between 140.8E°-141.2E°. The overall balance between these regions

300 results in no clear difference between locations receding and prograding in Table 1 and Figure 6b.

301 The strong positive trend in wave energy flux is maintained east of Cape Bridgewater (segment

302 (c), Figures 3c) with small counter-clockwise rotation of the mean wave direction (Figure 4c).

303 Along this extended region of the coast to Cape Otway (141.6E°-143.6E°), the coastline shows

304 small recession (approximately -0.1m/year – 3m over the measurement period of 30 years). East

305 of Cape Otway, the magnitude of the recession decreases and the shoreline shows little net change

306 in location. This behaviour is consistent with the reduced impact of south-westerly swell east of

307 Cape Otway, which provides some shelter from such waves. Table 1 and Figure 6c show that

308 summed across the full segment (c), a total of 53% of locations are receding and only 27%

309 prograding.

310 East of Cape Otway, the wave energy flux climate near the coast decreases (Figure 2b), as Cape

311 Otway provides protection from the south-westerly swell and $\Delta C_g E$ also decreases as the

312 protection provided by Tasmania becomes important (Figure 3d). The shoreline trends, ΔC_{GA}, are

313 complicated by the presence of Port Phillip Bay (Figures 3d, 4d). From Cape Otway to Inverloch

314 (143.6E°- 145.8E°) there is relatively little change in ΔC_{GA}. The relatively small region from

315 Inverloch to Wilson's Promontory (145.8E° - 146.4E°) shows a receding shoreline, previously

316 noted in studies of the area (Leach, et al., 2023). As a result, there is no clear overall differences

317 between recession and progradation for this section (Table 1 and Figure 6d). However, if one

318 considers just the ocean beaches (exclude Port Phillip Bay in Figures 3d and 4d), then there is

319 small recession along the entire coastline of section (d).

320 East of Wilson's Promontory the coastline is characterized by very long beaches and barrier islands

321 (Ninety-mile beach). This region from 147E° to 149.6E° (Wilson's Promontory to Cape Howe)

322 (Figures 3e-f, 4e-f) is characterized by a large counter-clockwise rotation of the mean wave

323 direction. The region immediately east of Wilson's Promontory (146.5°E – 147°E) shows strong

324 progradation. The remainder of this extended coastline, however, shows consistent recession of

325 approximately -0.5m/year (15m over the measurement period), particularly for section (f). This

326 section shows the strongest recession of any extended section, with Table 1 showing 60% of

327 locations receding and only 30% prograding. As noted above, the dominant swell in this region is

328 from the south-east and, although the changes in wave energy flux are small, there has been a

329 significant counter-clockwise rotation of the wave direction over the study period. This results in

330 the wave direction gradually becoming more shore-parallel. Therefore, the shoreline change noted

331 above is consistent with an increase in longshore drift (east to west) with sediment being

accumulated to the east of Wilson's Promontory. We should also note that this area east of Wilson Promontory is one of the few estuarine environments along the entire Victorian coast and hence some of the observed progradation may be due to fluvial deposits and ebb-tide delta formation (Konlechner, et al., 2020).

The results above use the percentage of coastal locations prograding or receding as the measure of whether the beach is responding to long term changes in waves and/or storm surge. As such, it does not consider the magnitudes of the progradation or recession. Figure 6 shows histograms of the magnitudes of the progradation/recession rates for each coastal sections. The figure confirms the results above showing sections (c) 142E° – 144E° and (f) 148E° – 150E° are clearly receding with other sections less clear, as explained for each section above.

In the above analysis, we speculate that changes in wave energy flux, $\Delta C_g E$ and mean wave direction, $\Delta \theta$ are the primary drivers of the observed changes in shoreline. The observed data supports this speculation. The Supplementary Material shows plots similar to Figures 3 and 4 for changes in the other related quantities: significant wave height, ΔH_s (Figures S1 a-c and S1 d-f), extreme significant wave height, ΔH_s^{95} (Figures S2 a-c and S2 d-f), mean wave period, ΔT_m (Figures S3 a-c and S3 d-f) and number of extreme wave events, $\Delta N_{H_s^{95}}$ (Figures S4 a-c and S4 d-f).

4. Discussion, conclusions and future work

Ghanavati, et al. (2023) found that at global scale, they could not distinguish a clear relationship between modelled (and observed) changes in wave energy flux and storm surge over the last 30 years and changes in shoreline position. The present dataset considers these relationships at higher resolution for the region of south-east Australia. This region is important in that it is an area with major spatial variations in wave energy flux climate (mean conditions) and some of the largest coastal trends in wave energy flux and mean wave direction globally in the last 30 years. In addition, both high resolution coastal wave and storm surge hindcasts are available, as well as high resolution observations of shoreline changes. As such, this is a unique region to determine if observable changes in shoreline position are evident as a consequence of long term changes in wave (and/or storm surge) climate.

The results show clear changes in shoreline position, which are consistent with postive trends in wave energy flux and changes in mean wave direction. In the western regions of the domain the mean wave direction is from the south-west and there have been positive trends in wave energy flux, $\Delta C_g E$ of approximately 14% (6/43kW/m). This appears to have resulted in non-stationary longshore drift from west to east and shoreline changes of approximately 3m over the 30 year study period.

In the central regions of the study domain both the mean wave energy flux and trends in wave energy flux decrease, as the island of Tasmania provides protection from the south-westerly swell. In this region there are no consistent trends in shoreline position with a similar number of coastal locations receding and prograding. Although ocean beaches do show small recession.

To the eastern end of the study domain, the protection provided by Tasmania and the deepwater conter-clockwise rotation of the mean wave climate means that the wave shadow of Tasmania results in a relatively large counter-clockwise rotation of the mean wave direction (up to 6° over the last 30 years). These changes in mean wave direction appear to be driving non-stationary behaviour of the beach systems in the region with the coastline from 146° to 149° (approximately 300 km) receding by up to 30m over the 30 year study period.

The results presented in this analysis are consistent with a study of this same region by Konlechner, et al. (2020) using lower resolution shoreline change data (Luijendijk, et al., 2018). The shoreline change "hot-spots" of that study are consistent with the present results. The results of the present study are also consistent with the global findings of Ghanavati, et al. (2023). Here, we find that long term changes in wave climate can apparently drive long-term changes in beach location but that relatively large changes in wave energy flux and/or direction are required to produce measurable changes in beach position. As noted, the study region has both a very energetic wave climate and some of the largest trends in this climate of any coastline. However, even in a region such as this, where long-term changes in wave energy flux are relatively large, the resulting changes in beach location are only approximately 1.0 m/year or 30m over the study period.

In the present analysis, we speculate that the observed changes in shoreline position in the western section of the domain are driven by non-stationary longshore drift from west to east with sediment transport being intercepted by Cape Bridgewater. Such behaviour is consistent with the observed increases in wave energy flux and the predominately south-westerly swell. In the eastern sections of the domain, we speculate that there is sediment transport from the east to west, intercepted by Wilson's Promontory. This speculation is consistent with the predominately south-easterly swell in the region and the observed counter-clockwise change in mean wave direction over the study period.

Although such speculation is consistent with the datasets, other processes may also have an impact on shoreline change. The most obvious such change is sea level rise, which could be expected to cause shoreline recession. Observations (Watson, et al., 2015; Nerem, et al., 2018) indicate that in recent years sea level rise in the Australia region has been approximately 3mm/year. The bed slope along the south-eastern coast of Australia is on average approximately 1:100 (Athanasiou, et al., 2019). Therefore, application of Bruun's rule (Bruun, 1962) would suggest a uniform recession of approximately 0.3 m/year. Such a value is smaller than, but comparable, to the observed recession in the western and eastern portions of the study domain. Recession due to sea level rise, however, would not account for the observed progradation west of Cape Bridgewater or east of Wilson's Promontory. In addition, Bishop-Taylor, et al. (2021) indicate that over their full dataset for

Australia, approximately the same number of beaches are receding (11.1%) as prograding (11.0%). Table 1 indicates that for the present study region this is also the case. Sea level rise would be expected to result in a net recession of beaches. In contrast non-equilibrium longshore drift driven by changes in wave climate will cause some beaches to recede whilst other prograde.

Therefore, we conclude that the present results are more consist with the impacts of changes in wave climate rather than sea level rise.

Although the present study is regional, it has global implications for the magnitude of changes in shoreline response which may result in other regions of the world under future projections of changes in wave climate. The present study clearly shows that impacts of changing wave climate will have strong regional characteristics and that it is important to consider the unique nature of each region in determining potential impacts. The response to individual coastal compartments will differ in terms of the magnitude of the response and even the sign (recession verses progradation).

As noted, the present analysis provides the first evidence of a causal relationship between long-term climate trends in waves and shoreline change. It does, however, have a number of limitations which should be addressed in future research. These future studies could include:

- Detailed sediment transport modelling to assess whether the observed changes in wave energy flux and wave direction would be expected to result in non-stationary longshore drift of the magnitude observed in the recorded shoreline position.

- The extraction of shoreline position from relatively low-resolution satellite images is computationally challenging. The Bishop-Taylor, et al. (2021) dataset represents a significant advance in resolution and accuracy. Further developments in the use of Artificial Intelligence approaches to determining shoreline postion are expected to further reduce errors in such data.

- The present analysis is limited to south-east Australia, as there were high-resolution datasets of long-term changes in waves, storm-surge and shoreline position available for this region. Dedicated projects modelling specific areas for the purpose of better determining the relationships between changes in these quantities would better quantify the likely impacts of future changes on vulnerable shoreline.

Code/Data availability

All data used in the paper and codes for the analysis are available from the authors upon request.

Competing Interests

The authors declare no competing interests.

Author Contributions

MG: Data curation, Investigation, Writing – original draft, Writing – review and editing; IY: Conceptualization, Investigation, Supervision, Writing – original draft, Writing – review and editing; EK: Writing – review and editing; JL: Writing – review and editing

References

Androulidakis, Y. S. et al., 2015. Storm surges in the Mediterranean Sea: variability and trends under future climatic conditions. *Dynamics of Atmospheres and Oceans,* Volume 71, pp. 56-82.

Athanasiou, P. et al., 2019. Global distribution of nearshore slopes with implications for coastal retreat. *Earth System Science Data,* Volume doi.org/10.5194/essd-2019-71.

Aydoğan, B. & Ayat, B., 2018. Spatial variability of long-term trends of significant wave heights in the Black Sea. *Applied Ocean Research,* Volume 79, pp. 20-35.

Barnard, P. et al., 2015. Coastal vulnerability across the Pacific dominated by El Niño/Southern Oscillation. *Nature Geosciences,* Volume 8, p. 801–807.

Bishop-Taylor, R., Nanson, R., Sagar, S. & Lymburner, L., 2021. Mapping Australia's dynamic coastline at mean sea level using three decades of Landsat imagery. *Remote Sens. Environ.,* Volume 267, p. 112734.

Bruun, P., 1962. Sea-Level Rise as a Cause of Shore Erosion. *Proc. American Society of Civil Engineers.*

Cao, Y., Dong, C., Young, I. & Yang, Y., 2021. Global wave height slowdown trend during a recent global warming slowdown. *Remote Sensing,* Volume 13, p. 4096.

Cid, A. et al., 2016. Long-term changes in the frequency, intensity and duration of extreme storm surge events in southern Europe.. *Climate Dynamics,* 46(5), p. 1503–1516.

Colberg, F., McInnes, K., O'Grady, J. & Hoeke, R., 2018. CSIRO Australia Coastal Sealevel Simulations. v1. CSIRO. Data Collection. p. https://doi.org/10.4225/08/5a7280a3a0d2a.

Egbert, G. D. & Erofeeva, S. Y., 2002. Efficient inverse modeling of barotropic ocean tides. *J. Atmos. and Ocean. Tech.,* Volume 19, p. 183–204.

Erikson, L. et al., 2022. Global ocean wave fields show consistent regional trends between 1980 and 2014 in a multi-product ensemble. *Comms. Earth & Env.,* Volume 3, p. 320.

Feng, J. et al., 2018. Storm surge variation along the coast of the Bohai Sea. *Scientific Reports,* 8(1), pp. 1-10.

474 Ghanavati, M. et al., 2023. An assessment of whether long-term global changes in waves and
475 storm surges have impacted global coastlines. *Scientific Reports,* Volume 13, p. 11549.

476 Harley, M. D. et al., 2017. Extreme coastal erosion enhanced by anomalous extratropical storm
477 wave direction. *Sci. Rep.,* Volume 7, p. 6033.

478 Harley, M., Turner, I., Short, A. & Ranasinghe, R., 2011. A re-evaluation of coastal embayment
479 rotation: The dominance of cross-shore versus alongshore sediment transport processes,
480 Collaroy-Narrabeen Beach, southeast Australia. *Jnl. Geophys. Res. (Earth Surface),* Volume
481 116.

482 Hemer, M., 2010. Historical trends in Southern Ocean storminess: Long-term variability of
483 extreme wave heights at Cape Sorell, Tasmania. *Geophys. Res. Lett.,* Volume 37, p. L18601.

484 Hemer, M. et al., 2013. Projected changes in wave climate from a multi-model ensemble. *Nature*
485 *Clim. Change,* Volume 3, pp. 471-476.

486 Hersbach, H. et al., 2020. The ERA5 global reanalysis. *Q. J. R. Meteorol. Soc.,* Volume 146, pp.
487 1999-2049..

488 Hinkel, J. et al., 2013. A global analysis of erosion of sandy beaches and sea-level rise: An
489 application of DIVA. *Global and Planetary Change,* Volume 111, pp. 150-158.

490 Hochet, A. et al., 2021. Sea state decadal variability in the North Atlantic: a review. *Climate,*
491 Volume 9, p. 173.

492 Kim, D. Y. et al., 2017. Sea Level Rise and Storm Surge around the Southeastern Coast of
493 Korea.. *Journal of Coastal Research,* 79(10079), pp. 239-243.

494 Komar, P., 1998. *Beach Processes and Sedimentation.* 544pp ed. s.l.:Prentice Hall.

495 Konlechner, T. et al., 2020. Mapping spatial variability in shoreline change hotspots from
496 satellite data; a case study in southeast Australia. *Estuarine, Coastal and Shelf Science,* Volume
497 246, p. 107018.

498 Leach, C. et al., 2023. Measuring drivers of shoreline and subaerial beach change using limited
499 datasets in a temperate, wave-dominated sandy system: Inverloch, Australia. *Ocean Coastal*
500 *Managment,* Volume 240, p. 106641.

501 Liu, J. et al., 2022. The wave climate of Bass Strait and south-east Australia. *Ocean Modelling,*
502 Volume 172, p. 101980.

503 Liu, J. et al., 2023. A high-resolution wave energy assessment of south-east Australia based on a
504 40-year hindcast. *Renewable Energy,* Volume 215, p. 118943.

505 Liu, J., Meucci, A. & Young, I., 2022. Projected wave climate of Bass Strait and south-east
506 Australia by the end of the twenty-first century. *Climate Dynamics,* pp. 10.1007/s00382-022-
507 06310-4.

508 Liu, J., Meucci, A. & Young, I., 2023. Projected 21st Century Wind-Wave Climate of Bass Strait
509 and South-East Australia: Comparison of EC-Earth3 and ACCESS-CM2 Climate Model
510 Forcing. *Jnl. Geophys. Res.,* Volume 128, p. e2022JC018996.

511 Liu, Q., Babanin, A., Rogers, E. & Zieger, S., 2021. Forty years of global wave hindcasts using
512 the observation-based source terms: validation and geophysical applications. *Journal of*
513 *Advances in Modeling Earth Systems,* 13(8).

514 Luijendijk, A. et al., 2018. The state of the world's beaches. *Scientific Reports,* Volume 8, pp. 1-
515 11.

516 Masselink, G. et al., 2016. Extreme wave activity during 2013/2014 winter and morphological
517 impacts along the Atlantic coast of Europe. *Geophy. Res. Lett.,* Volume 43, p. 2135–2143.

518 Meucci, A., Young, I., Hemer, M. K. E. & Ranasinghe, R., 2020. Projected 21st century changes
519 in extreme wind-wave events. *Science Advances,* 6(24), p. eaaz7295.

520 Meucci, A. et al., 2023. 140 Years of Global Ocean Wind-Wave Climate Derived from CMIP6
521 ACCESS-CM2 and EC-Earth3 GCMs: Global Trends, Regional Changes, and Future
522 Projections. *Jnl. Climate,* Volume 36, pp. 1605-1631.

523 Meucci, A. et al., 2023. Evaluation of spectral wave model physics as applied to a 100-year
524 Southern Hemisphere extra tropical-cyclone sea state. *J. Geophys. Res. Oceans,* Volume 128, p.
525 e2022JC018996.

526 Morim, J. et al., 2022. A global ensemble of ocean wave climate statistics from contemporary
527 wave reanalysis and hindcasts. *Scientific Data,* Volume 9, p. 358.

528 Morim, J. et al., 2023. Understanding uncertainties in contemporary and future extreme wave
529 events for broad-scale impact and adaptation planning. *Science Advances,* Volume 9, p.
530 eade3170.

531 Muis, S. et al., 2016. A global reanalysis of storm surges and extreme sea levels. *Nat. Commun.,*
532 Volume 7, p. 11969.

533 Nerem, R. et al., 2018. Climate-change–driven accelerated sea-level rise detected in the altimeter
534 era. *Proc. National Academy of Sciences,* Volume 115, p. 2022–2025.

535 Paprotny, D., 2014. Trends in storm surge probability of occurrence along the Polish Baltic Sea
536 coast.. *arXiv preprint arXiv.*

537 Ranasinghe, R., 2016. Assessing climate change impacts on open sandy coasts: A review. *Earth-*
538 *Science Reviews,* Volume 160, pp. 320-332.

539 Ranasinghe, R., R., M., A., S. & G., S., 2004. The Southern Oscillation Index, Wave Climate,
540 and Beach Rotation. *Marine Geology,* pp. 273-287.

541 Ranasinghe, R. et al., 2021. Climate change information for regional impact and for risk
542 assessment. . In: *Climate Change 2021: The Physical Science Basis. Contribution of Working*

Group 1 to the Sixth Assessment Report of the Intergovernmental Panel on Climate Change. Cambridge: Cambridge University Press, pp. 1767-1926.

Reguero, B. G., Losada, I. J. & Méndez., F. J., 2019. A recent increase in global wave power as a consequence of oceanic warming.. *Nature communications,* pp. 1-14.

Saha, S. et al., 2010. The NCEP Climate Forecast System Reanalysis. *B. Am. Meteorol. Soc.,* Volume 91, p. 1015–1057.

Sen, P., 1968. Estimates of the regression coefficient based on Kendals TAU. *Amer. Stats. Assoc. Journal,* pp. 1379-1389.

Shchepetkin, A. F. & McWilliams, J. C., 2005. The regional oceanic modeling system (ROMS): a split-explicit, free-surface, topography-following-coordinate oceanic model. *Ocean Modeling,* Volume 9, p. 347–404.

Takbash, A. & Young, I., 2020. Long-term and seasonal trends in global wave height extremes derived from ERA-5 reanalysis data. *J. Mar. Sci. & Eng.,* Volume 8, p. 1015.

Timmermans, B., Gommenginger, C., Dodet, G. & Bidlot, J.-R., 2020. Global Wave Height Trends and Variability from New Multimission Satellite Altimeter Products, Reanalyses, and Wave Buoys. *Geophys. Res. Lett.,* Volume 47, p. e2019GL086880..

Vitousek, S. et al., 2023. A model integrating satellite-derived shoreline observations for predicting fine-scale shoreline response to waves and sea-level rise across large coastal regions. *Jnl. Geophys. Res. Earth Surface,* p. e2022JF006936.

Vos, K., Harley, M., Turner, I. & Splinter, K., 2023. Pacific shoreline erosion and accretion patterns controlled by El Niño/Southern Oscillation. *Nature Geoscience,* Volume 16, p. 140–146.

Vousdoukas, M. et al., 2020. Economic motivation for raising coastal flood defenses in Europe. *Nature Comms.,* Volume 11, p. 2119.

Wang, X. L. & Swail, V. R., 2001. Changes of extreme wave heights in northern hemisphere oceans and related atmospheric circulation regimes. *J. Clim.,* pp. 2204-2221.

Wang, X. L. et al., 2009. Detection of external influence on trends of atmospheric storminess and northern oceans wave heights.. *Clim. Dyn. ,* pp. 189-203.

Watson, C. et al., 2015. Unabated global mean sea-level rise over the satellite altimeter era. *Nature Climate Change,* Volume 5, p. 565–568.

Young, I. & Ribal, A., 2019. Multi-platform evaluation of global trends in wind speed and wave height. *Science,* Volume 364, pp. 548-552.

Young, I. & Ribal, A., 2022. Can multi-mission altimeter datasets accurately measure long-term trends in wave height. *Rem. Sens.,* Volume 14, p. 974.

Young, I., Zieger, S. & Babanin, A., 2011. Global trends in wind speed and wave height. *Science,* Volume 332, pp. 451-455.

578 Zheng, C. W. & Li, C. Y., 2017. Analysis of temporal and spatial characteristics of waves in the
579 Indian Ocean based on ERA-40 wave reanalysis,. *Applied Ocean Research,* Volume 63, pp. 217-
580 228.

581

582

583

584

Tables and Figures

586

Coastal Segment	Recession (-0.05 to -1m/yr)	Progradation (+0.05 to +1m/yr)	Stable (-0.05 to +0.05m/yr)
(a) 138°-140°	40%	45%	15%
(b) 140°-142°	40%	46%	14%
(c) 142°-144°	53%	27%	20%
(d) 144°-146°	37%	49%	14%
(e) 146°-148°	40%	50%	10%
(f) 148°-150°	60%	30%	10%

587

588 Table 1: Percentage of coastal locations, as defined by the Bishop-Taylor, et al. (2021) dataset
589 receding (-0.05 to -1.00m/year), prograding (+0.05 to +1.00m/year) or stable ($\pm$ 0.05m/year)
590 over the period 1988 to 2013.

591

593 Figure 1: The coastal region of south-east Australia comprising the study area. For analysis
594 purposes the region is divided into six sections: (a) 138°-140°, (b) 140°-142°, (c) 142°-144°, (d)
595 144°-146°, (e) 146°-148° and (f) 148°-150° from west to east. The island of Tasmania is to the
596 south of this coastline. (© Google Maps)

597
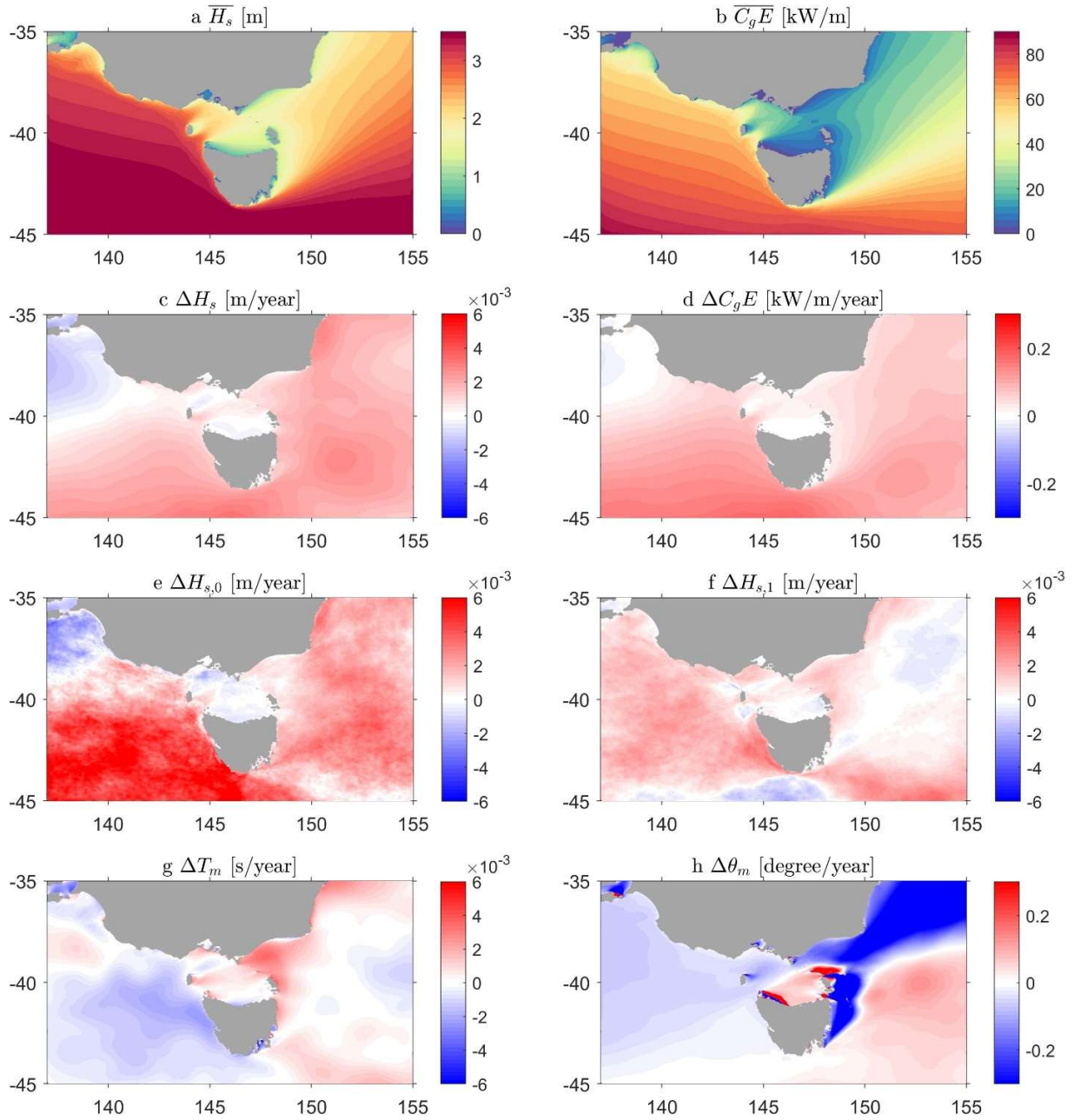
Figure 2: Wave climate and trends in the study region of south-eastern Australia over the period 1988 to 2013 as modelled by the Liu, et al. (2022) regional wave model. (a) mean significant wave height, (b) mean wave energy flux, (c) trend in significant wave height, (d) trend in wave energy flux, (e) trend in wind-wave portion of the spectrum, (f) trend in swell portion of the spectrum, (g) trend in mean wave period, (h) trend in mean wave direction.

604
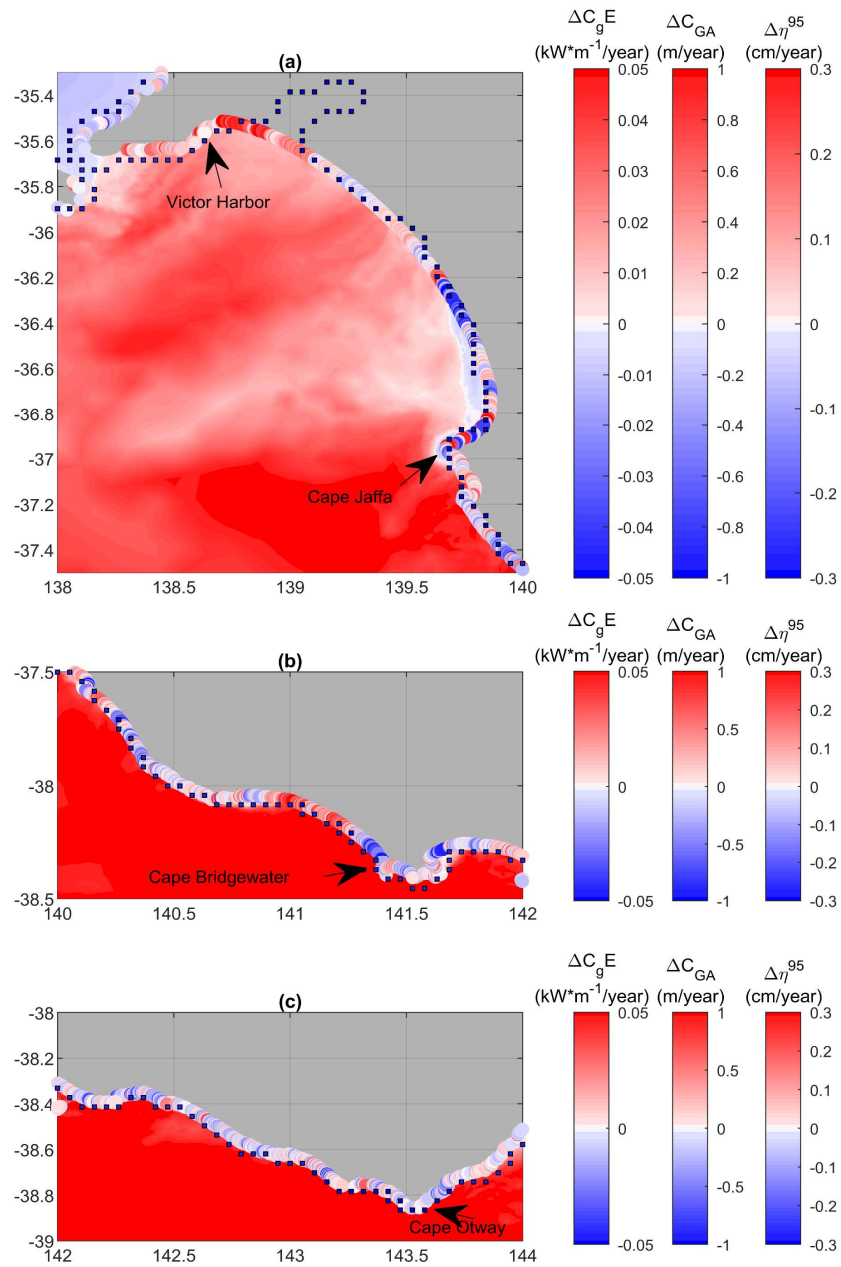
Figure 3 a-c: Trends in: wave energy flux, $\Delta C_g E$ shown as colour shaded values over the
domain, storm surge, $\Delta \eta^{95}$ shown as colour shaded squares at coastal model locations and
shoreline progradation/recession, ΔC_{GA} shown as colour shaded circles at beach locations.
Results shown for sections (a) 138E°-140E°, (b) 140E°-142E°, (c) 142E°-144E°.
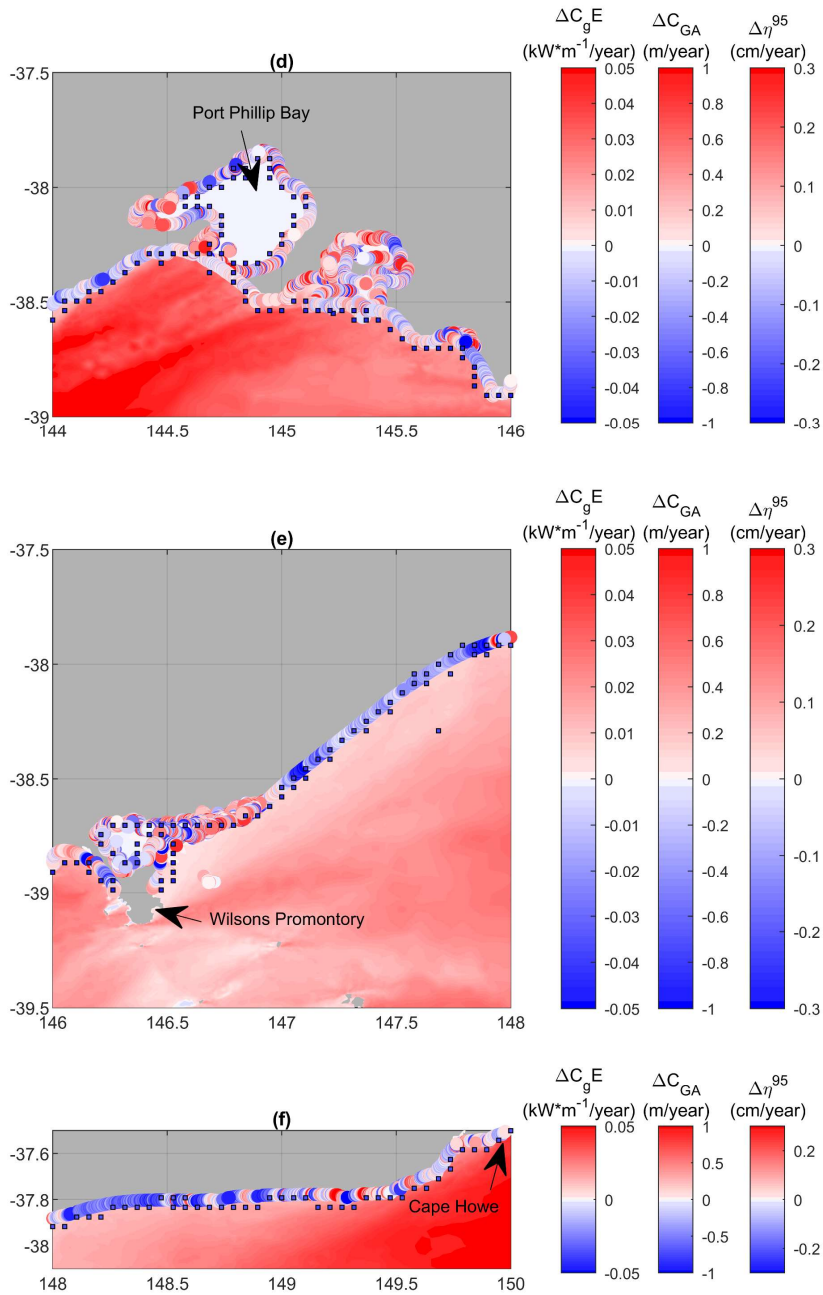
618   Figure 3 d-f: Trends in: wave energy flux, $\Delta C_g E$ shown as colour shaded values over the

619   domain, storm surge, $\Delta \eta^{95}$ shown as a colour shaded squares at coastal model locations and

620   shoreline progradation/recession, ΔC_{GA} shown as colour shaded circles at beach locations.

621   Results shown for sections (d) 144E°-146E°, (e) 146E°-148E° and (f) 148E°-150E°.

622

623
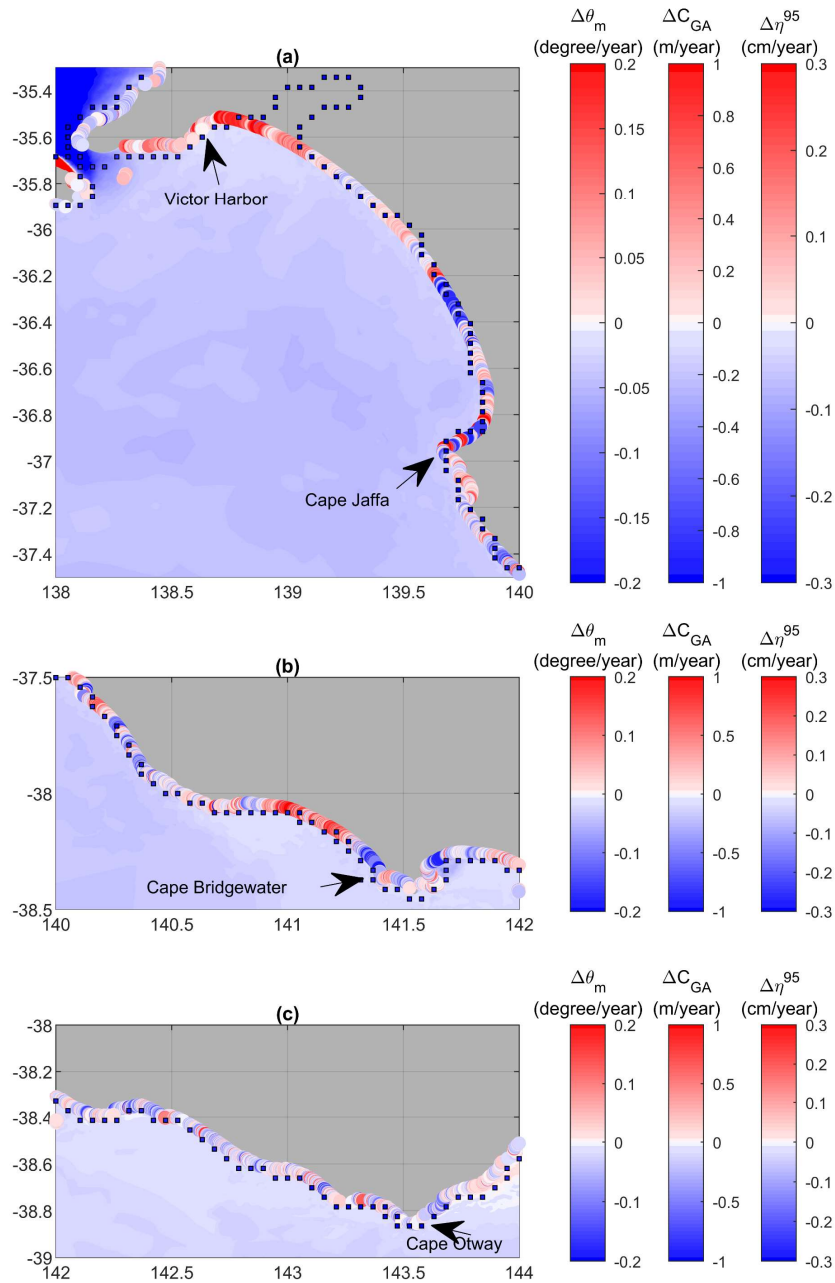
Figure 4 a-c: Trends in: mean wave direction, $\Delta\theta_m$ shown as colour shaded values over the domain, storm surge, $\Delta\eta^{95}$ shown as colour shaded squares at coastal model locations and shoreline progradation/recession, ΔC_{GA} shown as colour shaded circles at beach locations. Results shown for sections (a) 138E°-140E°, (b) 140E°-142E°, (c) 142E°-144E°.

633
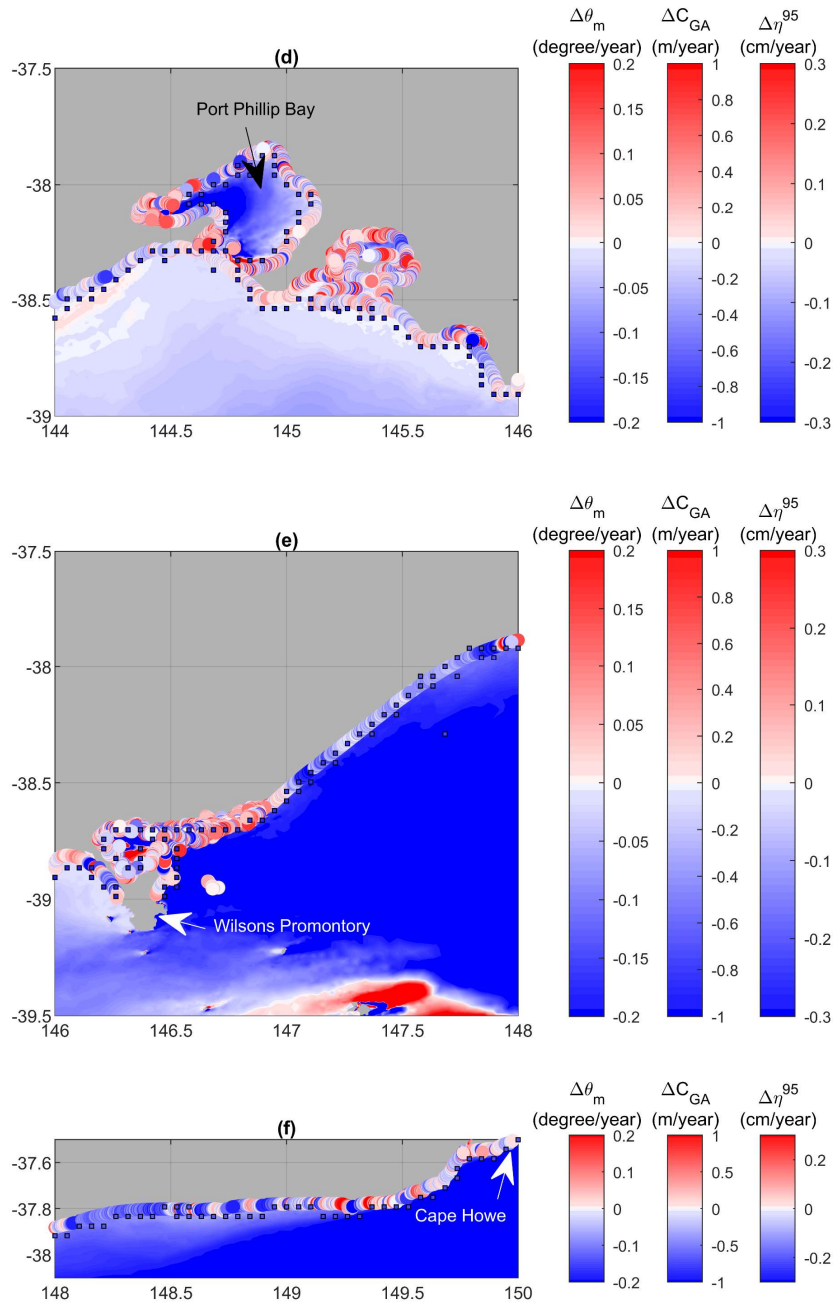
Figure 4 d-f: Trends in mean wave direction, $\Delta\theta_m$ shown as colour shaded values over the domain, storm surge, $\Delta\eta^{95}$ shown as a colour shaded squares at coastal model locations and shoreline progradation/recession, ΔC_{GA} shown as colour shaded circles at beach locations. Results shown for sections (d) 144E°-146E°, (e) 146E°-148E° and (f) 148E°-150E°.
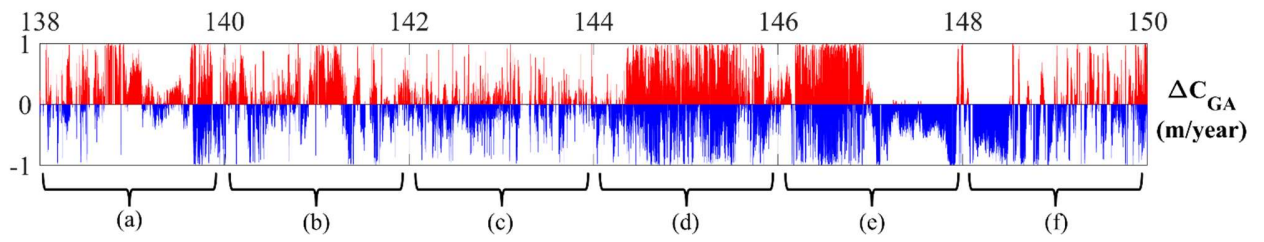
638

639  Figure 5: Bar chart showing values of progradation (red) and recession (blue), ΔC_{GA} at each

640  coastal location of the Bishop-Taylor, et al. (2021) dataset. Values are shown as a function of the

641  longitude (horizonal axis) and units are m/year. The regions shown in Figure 1 are labelled (a) to

642  (f).
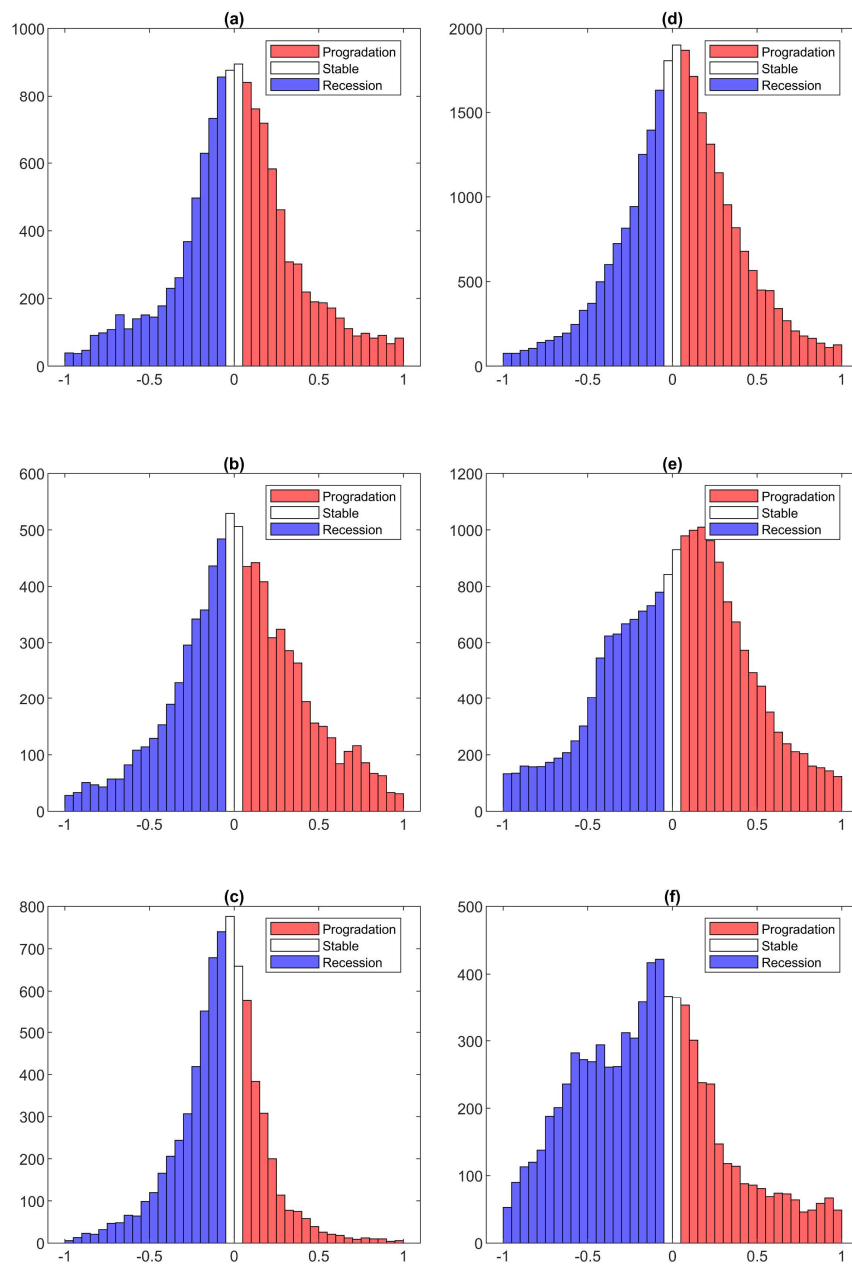
Figure 6: Histograms of progradation/recession rates for each of the coastal sections over the period 1988 to 2013. (a) 138E°-140E°, (b) 140E°-142E°, (c) 142E°-144E°, (d) 144E°-146E°, (e) 146E°-148E° and (f) 148E°-150E° from west to east.

655